Deep ice as a geochemical reactor: insights from iron speciation and mineralogy of dust in the Talos Dome ice core (East Antarctica)

Giovanni Baccolo[1,2], Barbara Delmonte[1], Elena Di Stefano[1,2,3], Giannantonio Cibin[4], Ilaria Crotti[5,6], Massimo Frezzotti[7], Dariush Hampai[8], Yoshinori Iizuka[9], Augusto Marcelli[8,10], and Valter Maggi[1,2]

[1]Environmental and Earth Science Department, University Milano-Bicocca, Italy
[2]Istituto Nazionale di Fisica Nucleare, section of Milano-Bicocca, Milan, Italy
[3]Department of Physical, Earth and Environmental Sciences, University of Siena, Italy
[4]Diamond Light Source, Harwell Science and Innovation Campus, Didcot, UK
[5]Department of Environmental Sciences, Informatics and Statistics, Ca' Foscari University of Venice, Italy
[6]Laboratoire des Sciences du Climat et de l'Environnement IPSL/CEA-CNRS-UVSQ UMR, Gif-sur-Yvette, France
[7]Department of Science, University Roma Tre, Italy
[8]Istituto Nazionale di Fisica Nucleare, Laboratori Nazionali di Frascati, Frascati, Italy
[9]Institute of Low Temperature Science, Hokkaido University, Sapporo, Japan
[10]Rome International Center for Materials Science - Superstripes, Rome, Italy

Correspondence to: Giovanni Baccolo (giovanni.baccolo@unimib.it)

Abstract. Thanks to its insolubility, mineral dust is considered a stable proxy in polar ice cores. With this study we show that the Talos Dome ice core (TALDICE, Ross Sea sector of East Antarctica) displays evident and progressive signs of post-depositional processes affecting the mineral dust record below 1000 m deep. We apply a suite of established and cutting-edge techniques to investigate the properties of dust in TALDICE, ranging from concentration and grain-size to elemental-composition and Fe-mineralogy. Results show that through acidic/oxidative weathering, the conditions of deep ice at Talos Dome promote the dissolution of specific minerals and the englacial formation of others, affecting dust primitive features. The expulsion of acidic atmospheric species from ice-grains and their concentration in localized environments is likely the main process responsible for englacial reactions. Deep ice can be seen as a "geochemical reactor" capable of fostering complex reactions which involve both soluble and insoluble impurities. Fe-bearing minerals can efficiently help exploring such transformations.

1. Introduction

Antarctic ice cores are a valuable archive which allows to reconstruct the climatic history of the Earth during the last 800.000 years (Wolff et al., 2010). Mineral dust is one of the most extensively studied proxies in ice cores. Its importance stems from its role in the Earth's climate system: production, transport and deposition of dust are controlled by climate-related processes, but at the same time dust affects the climate (Maher et al., 2010). Studying the properties of dust trapped in ice cores, it is possible to obtain information on how the climate influences the dust cycle (Delmonte et al., 2004) and about the effects of dust under different climatic regimes (Mahowald et al., 1999; Wolff et al., 2006; Potenza et al., 2016).

1

It is known that the physical and compositional properties of dust trapped in ice cores are influenced by climatic, environmental and atmospheric processes (Sugden et al., 2009; Delmonte et al., 2017; Markle et al., 2018). The dust concentration in ice is strictly controlled by climate (Delmonte et al., 2002), dust grain size is related to its atmospheric transport (Delmonte et al., 2017; Albani et al., 2012a) and geochemistry to dust sources (Delmonte et al., 2004).

Recently, a growing number of studies focused on the preservation and decay of climatic proxies in ice cores over time (Barnes et al., 2003; De Angelis et al., 2013; Ohno et al., 2016; Eichler et al., 2019; Baccolo et al., 2021). After the incorporation in snow, the proxies are affected by alterations produced by post-depositional processes. Generally, the influence of such changes progressively increases with ice age and depth (De Angelis et al., 2013; Tison et al., 2015). Post-depositional processes in deep ice are related to three main causes: (1) the interaction between ice flow and bedrock (Goossens et al., 2016); (2) the metamorphism of ice, intended as the set of physical transformations to which ice is subject at increasing pressure and age (Faria et al., 2010); 3- the diffusion of impurities (Barnes et al., 2003). An irregular bedrock can produce stratigraphic disturbances affecting the original ice succession for several hundred meters. On the contrary, ice metamorphism and englacial diffusion act at ice-crystal scale (mm-cm scale) (Rempel et al., 2002; Faria et al., 2010). The effects of such phenomena on the proxies investigated in ice cores are not yet fully understood, but improving their comprehension is essential considering the "Oldest Ice" challenge (Fischer et al., 2013).

Dust is considered relatively immobile and stable in ice and its concentration is used to synchronize deep ice cores when other proxies are deteriorated (Ruth et al., 2007; Kawamura et al., 2017). However, mineral particles may be altered by post-depositional changes. Impurities in ice are affected by small-scale relocation resulting from ice metamorphism, i.e. the re-crystallization and orientation of ice grains (Faria et al., 2010; Marath and Wettlaufer, 2020). Being most of the impurities incompatible with respect to the ice lattice (Wolff, 1996), during the re-crystallization the impurities are expulsed from the ice crystalline structure and accumulated at ice grain junctions or within intra-grain micro-inclusions (Mulvaney et al., 1988; De Angelis et al., 2005; Sakurai et al., 2017; Stoll et al., 2021). The accumulation of soluble and insoluble impurities forms eutectic mixtures whose pressure melting point is below the ice temperature, promoting the localized formation of liquid brines which lead to *in situ* chemical reactions (Fukazawa et al., 1998; De Angelis et al., 2005, 2013; Sakurai et al., 2017). Such small scale environments are dominated by sulphur-rich acidic species, strongly affected by re-mobilization and concentration because of their high incompatibility with the ice lattice (Mulvaney et al., 1988; Wolff, 1996; Fukazawa et al., 1998). The interaction between acidic brines and concentrated impurities, including dust, leads to acid-base reactions (Traversi et al., 2009; Ohno et al., 2016). Considering dust, the most common reactions happening in ice are the dissolution of carbonates, the precipitation of gypsum (Ohno et al., 2006; Iizuka et al., 2008; Eichler et al., 2019) and of other uncommon sulphates (Ohno et al., 2014), and the englacial formation of secondary iron minerals (De Angelis et al., 2013; Baccolo et al., 2021). Below 3000 m deep in the EPICA Dome C ice core, also the re-precipitation of carbonates has been reported, suggesting that once acidity is consumed, additional reactions take place (Tison et al., 2015).

65 The iron fraction of dust is particularly sensitive to englacial transformations. De Angelis et al. (2013) have identified secondary Fe-bearing minerals in the deep part of the EPICA Dome C ice core, while Eichler et al. (2019) have detected in the EPICA Dronning Maud Land ice core a few particles with a Raman signature compatible with jarosite, a Fe-K sulphate forming from mineral weathering (Papike et al., 2006). This finding is confirmed by a thorough investigation of the Talos Dome ice core (TALDICE, East Antarctica), where jarosite is found below 1000 m deep and interpreted as the result of
70 acidic, water-limited weathering of dust (Baccolo et al., 2021). Since Fe biogeochemistry is strongly coupled with the global carbon cycle, this element receives considerable attention by the ice core community (Wolff et al., 2006; Conway et al., 2015; Hooper et al., 2019) and methods have been developed to measure its concentration and speciation (Spolaor et al., 2013; Burgay et al., 2019). Nevertheless, the effects of post-depositional processes in ice cores on its geochemistry are still poorly investigated.

75 This work presents and discusses a set of geochemical evidences showing that below 1000 m deep the dust record of TALDICE is affected by post-depositional transformations which alter its particle-size distribution, elemental composition, and mineralogy. A detailed analysis of speciation and mineralogy of the Fe-fraction of dust reveals that deep ice at Talos Dome acts as a geochemical reactor, favoring reactions and transformations which involve both soluble and insoluble impurities.

80 ## 2. Materials and methods

2.1. The TALDICE ice core

TALDICE has been drilled at Talos Dome (72°490S, 159°110E; 2315 m a.s.l., Fig.1), a peripheral ice dome in the Ross Sea sector of East Antarctica (Frezzotti et al., 2004). It is 1620 m long and its ice age at 1438 m deep (depth refers to the distance between the ice surface and the considered section of the core) is ~150 ky BP according to the AICC2012 chronology (Veres
85 et al., 2013; Bazin et al., 2013), but there is evidence that the water stable isotope record is preserved up to ~1550 m deep, where the estimated ice age is ~343 ky BP, corresponding to Marine Isotopic Stage 10.1 (Crotti et al., 2021). Dust concentration in TALDICE during the last climatic cycle reflects high atmospheric loads in glacial periods and lower ones during interglacials, as observed at other East Antarctic sites (Delmonte et al., 2010). A peculiarity of TALDICE is given by the influence of local Antarctic dust sources, corresponding to the ice-free sites of the Victoria Land region, close to Talos
90 Dome (Albani et al., 2012a; Baccolo et al., 2018b).

2.2. Sample preparation

Fifty-four samples are prepared using 191 TALDICE ice sections (~25x3x2 cm). They consist of insoluble mineral particles extracted from meltwater and deposited on filtration membranes. The preparation takes place in a clean room (ISO6)

installed at the University of Milano-Bicocca. Ice sections are decontaminated with three baths in ultra-pure MilliQ water
(Merck Millipore). They are stored in clean tubes under a ISO5 laminar flow bench until melted. Meltwater is split in two
aliquots, one (~10 mL) for Coulter counter, the remnant for synchrotron radiation analysis.

The aliquots for Coulter counter (CC), corresponding to single ice sections, are stored in plastic cuvettes (rinsed with MilliQ
water) and added with a NaCl solution (final Na^+ concentration of samples ~1% m/m). The solution is prepared using MilliQ
water and high purity solid NaCl and before use it is filtered with 0.22 μm pore-size filters. This procedure makes liquid
samples electrically conductive, a requisite for CC. The aliquots for synchrotron radiation analysis are merged considering
multiple ice sections (191 in total), so as to prepare 54 samples with a total dust mass of at least 1 μg. Merged samples are
filtrated using hydrophilic PTFE membranes (ø 13 mm, pore-size 0.4 μm). Before filtration, membranes are rinsed for two
weeks in a high purity HNO_3 solution (concentration m/m 5%, weekly renewed). Filtration is done with a micro-pipette to
concentrate the particles on the membrane in the smallest possible area (Macis et al., 2018). After filtration the membranes
are placed in dedicated clean PTFE holders and sealed in plastic bags.

Seven samples correspond to the Holocene (0-673 m, 0-11.7 ky BP), 7 to the last deglaciation (674-827 m, 11.7-18 ky BP), 5
to MIS2 (828-951 m, 18-30 ky BP), 15 to MIS3 (952-1259 m, 30-60 ky BP), 2 to MIS4 (1260-1292 m, 60-80 ky BP), 6 to
MIS5 (1293-1418 m, 80-146 ky BP), 1 to MIS6 (1419-1438 m, 146 154 ky BP) and 11 to the deep part of TALDICE not
dated by AICC2012 chronology (1439-1620 m), but partially dated by the new deep chronology (Crotti et al., 2021).

2.3. Coulter counter

To determine the concentration and grain size of insoluble dust particles, CC is used. The method is well-known for the
analysis of insoluble particles in ice cores. It relates the changes in the electrical conductance of meltwater with the size and
number of insoluble particles suspended into the suspension (Delmonte et al., 2002). Samples are measured with a Beckman
Multisizer 4, equipped with a 30 μm orifice to measure the concentration of particles between 0.6 and 18 μm divided into
400 channels.

2.4. Synchrotron radiation spectroscopic measurements

The application of synchrotron light to determine the elemental and mineralogical composition of TALDICE dust is
performed at beamtime B18 of the Diamond Light source (Cibin et al., 2019). A glovebox is connected to the experimental
chamber of the beamline to handle the samples in clean conditions. Additional precautions are adopted to limit
contamination and increase the signal to noise ratio: the application of plastic sheets inside the experimental chamber to limit
radiation backscattering; the defocus of the incidental beam to illuminate the largest part of the samples; the preservation of
high-vacuum during the acquisition. Further details are available in Baccolo et al. (2018a).

2.4.1. X-ray fluorescence spectroscopy

Major elements in dust are investigated through X-ray fluorescence spectroscopy, using synchrotron radiation as the
125　excitation source (Iida, 2013). Samples are irradiated with a 10 keV beam (cross section ~1x1 mm) for 600 s and the
fluorescence signal is acquired with a silicon drift detector, allowing the quantification of the following elements: Na, Mg,
Al, Si, K, Ca, Ti, Mn, Fe. Analytical accuracy is evaluated analyzing NIST standard reference materials (SRM 2709a); it
decreases from light to heavy elements (standard deviation of the replicates for Na is 25%, 10% for Fe). Recovery factors are
evaluated comparing certified concentrations of SRMs with calculated values: they range from 85% to 115% except for Ca
130　and Na (133% and 129%). Full details are given in Baccolo et al. (2018a, b). Elemental concentrations are converted into
oxides concentrations and closed to 100% (Rudnick and Gao, 2003).

2.4.2. X-ray absorption spectroscopy

Speciation and mineralogy of the Fe fraction of TALDICE dust are investigated through X-ray absorption near edge
structure spectroscopy (XANES), performed at the Fe K-edge transition, that is the excitation energy of the innermost
135　electrons of Fe. XANES relates the spectral features of X-ray absorption spectra to chemical and molecular characteristics of
specific elements. The sample is irradiated with a monochromatic beam of photons whose energy finely changes with time.
The response of the sample depends on features such as oxidation, coordination and mineralogy (Calvin, 2013). For each
sample three measurements are carried out, acquiring the fluorescence signal of the samples at steps of 0.15 eV and
considering the interval between 7000 and 7400 eV. Spectra are calibrated, normalized and averaged using the Athena
140　software (Ravel and Newville, 2005). Three spectral features are gathered: (1) the energy of the Fe K-edge transition; (2) the
energy of the pre-edge peak centroid; 3- the intensity of the pre-edge peak (Fig. S1) (Baccolo et al., 2018b). The energy of
both pre-edge peak and Fe K-edge transition are directly related to the oxidation state of Fe, while the intensity of the pre-
edge peak depends on its coordination (Berry et al., 2003).

2.4.3. Relative abundance of Fe-bearing minerals

145　Comparing dust samples with the ones corresponding to 14 Fe-mineral references (biotite, chlorite, glaucophane, goethite,
hematite, hornblende (ferro-hornblende), jarosite, magnetite, muscovite, fayalite, pargasite, pyrite, schoerlite, siderite), it is
possible to estimate the contribution of single Fe-bearing minerals into the samples (Shoenfelt et al., 2018). XANES spectra
of minerals are collected following the protocol adopted for TALDICE samples (Fig. S2). XANES spectra of ice core dust
are reproduced through ordinary least square regression (OLS), using linear combinations constructed with mineral spectra
150　(Fig. S3). For each sample all the combinations defined by 4, 3, 2 and 1 mineral references (1456 combinations per sample)
are calculated through OLS and the best one (in terms of R-squared, it always exceeded 0.9) is selected to represent the
sample. In some cases, the second best-fit combination has an R-squared close to the best-fit, but the difference between the
two combinations always regards the less abundant of the 4 selected references, with negligible effects on the interpretation.

The combinatoric package of the Athena software is used (Ravel and Newville, 2005). Following the procedure adopted by Shoenfelt et al. (2018), the relative abundance of Fe-bearing minerals is estimated considering the % linear coefficients obtained from OLS.

3. Results and discussion

3.1. The TALDICE dust record

Considering the last climatic cycle (the Holocene and MIS 2-3-4), well-known features characterizing the relationships between the atmospheric dust cycle and Antarctic climate are visible (Fig. 1). The most evident is the negative correlation between dust concentration and $\delta^{18}O$. In accordance with the suppression of dust production and transport from remote sources during interglacials (Albani et al., 2012b), the mean dust concentration in TALDICE Holocene ice is ~25 ng g^{-1}, while during MIS2 it exceeds 300 ng g^{-1}, as a consequence of the activation of South American sources (Sugden et al., 2009) and the enhanced atmospheric transport toward Antarctica (Markle et al., 2018).

Such shift from interglacial to glacial conditions not only affects dust concentration, but also its grain size, as revealed by the fine particle percentage (FPP) and coarse local particle percentage (CLPP) indexes. The first one is the relative concentration of particles between 0.6 and 2 μm with respect to the 0.6 - 5 μm interval; CLPP is the ratio between the concentration of particles between 5 and 10 μm and the total concentration of particles between 0.6 and 10 μm. During the Holocene, FPP has a mean value of 50%, while during MIS2 it increases to 63%, revealing that under glacial conditions dust particles deposited at Talos Dome are smaller than in interglacial periods. Similar evidences have already been observed in other East Antarctic sites (Dome C, Vostok) and interpreted considering that dust transported to East Antarctica during glacials is subject to long-range and high-altitude atmospheric pathways, allowing the efficient removal of coarse particles (Delmonte et al., 2002). CLPP has a mean value of 19% during the Holocene and of 6.5% during MIS-2. This index is indicative of the relative abundance of particles larger than 5 μm, which are related to local Antarctic sources (Albani et al., 2012a; Baccolo et al., 2018b). The decrease of the index in glacial periods must be interpreted in relative terms. CLPP is lower in glacials not because of a reduction of coarse particles, but due to an increase of the fine ones from South America (Baccolo et al., 2018b).

MIS4 displays features similar to MIS2, while MIS5.5 is similar to the Holocene, confirming increased deposition of fine dust during glacial culminations and reduced fluxes of relatively coarse dust during peak interglacial warmth. In the deeper layers of the core, the relationship between dust and climate is less evident. Fig. 1 and Tab. 1 show that below 1430 m deep, dust concentration exceeds 100 ng g^{-1} with dampened oscillations. CLPP exceeds 20% and FPP drops below 45%, highlighting that in deep TALDICE dust particles are coarser. This can be interpreted as a consequence of dust aggregation in deep ice, a process already observed in Antarctic ice below 2500 m deep (Lambert et al., 2008; De Angelis et al., 2013).

Table 1. Dust concentration in TALDICE. For each climatic period mean concentrations are reported along with standard deviations.

Period	Holocene	Degl.	MIS2	MIS3	MIS4	MIS5	MIS6	MIS7	MIS8-9	deep part
(kyr BP)	0-11.7	11.7-19	19-31	31-58	58-68	68-132	132-190	190-246	246-337	337-unk.
Conc. (ng g^{-1})	26±18	104±25	317±174	80±31	116±59	61±55	158±190	182±302	121±73	110±123
FPP (%)	50±4	57±8	63±8	55±7	53±5	52±5	54±7	45±9	35±10	36±9
CLPP (%)	19±7	14±7	6.5±3.4	10±5	9.6±3.9	13±8	9.1±5.2	21±14	21±6	24±11

185
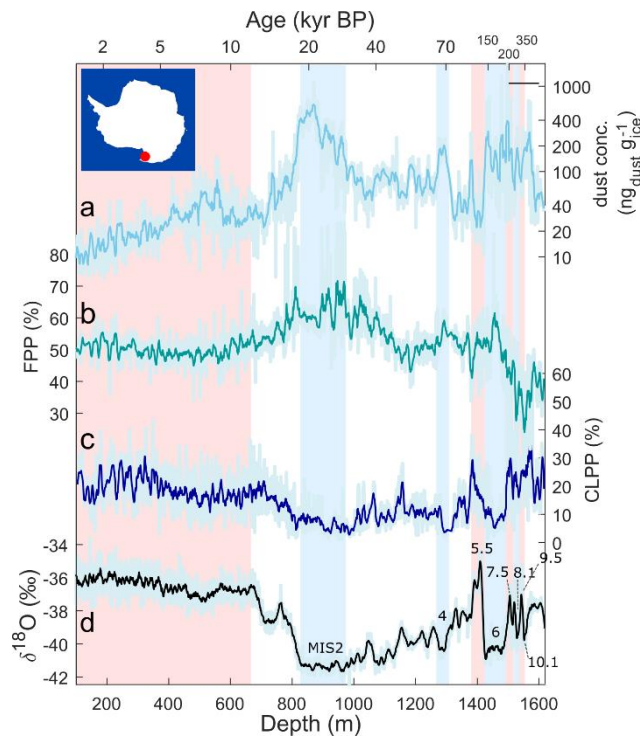
Figure 1. The mineral dust record of TALDICE. From the upper to the lower curve: (a) total dust concentration of insoluble particles (Baccolo et al., 2021); (b) FPP (fine particle percentage); (c) CLPP (coarse local particle percentage); (d) $\delta^{18}O$ (Stenni et al., 2011). Light blue bands highlight glacial culminations (MIS 2-4-6-8), the red bands the Holocene and MIS 5.5, 7.5 and 9.5. In the upper-left corner the position of Talos Dome in Antarctica.

Size distributions of insoluble particles also point to dust aggregation. Dust from the upper part of the core (Figure 2e-h), presents a mode between 1 and 2.5 µm and a tail of particles larger than 5 µm, suggesting a mix from remote and local sources (Albani et al., 2012a). Dust from deep TALDICE (Figure 2j-l) is characterized by a higher abundance of coarse particles, a lack of fine ones and modal values exceeding 4 µm. Such features are not encountered in shallow sections of

7

Antarctic ice cores, where the effects of post-depositional alterations are limited (Royer et al., 1983; Delmonte et al., 2002; Wegner et al., 2015); they result from *in situ* aggregation of particles in deep ice (Lambert et al., 2008; De Angelis et al., 2013; Baccolo et al., 2021).

Post-depositional processes in TALDICE ice also influence the climatic significance of the dust record. This is shown in Fig. 2a-d, where the correlation between dust and ice stable isotopes is analyzed. The correlation is high during the last climatic cycle, but decreases in older periods (R-squared decreases from 0.66 during the last cycle, to less than 0.3 in the deep core). The same conclusion is drawn looking at the trajectory describing the evolution of the $\delta^{18}O$ – dust pair. During the first cycle it well reproduces the transition from glacial to interglacial conditions, including the Antarctic Cold Reversal and the partition of the last glacial period into MIS 2-3-4. This is partially true for the previous climatic cycle, but the correlation decreases (R-squared from 0.66 to 0.49). The degradation continues in the deepest part of TALDICE, where the coefficient does not exceed 0.25 and the trajectories follow irregular paths, highlighting a substantial decoupling of dust concentration and isotopic signals. This is confirmed by Crotti and colleagues (2021) who showed that at Talos Dome below 1548 m deep, the climatic signals are not preserved.
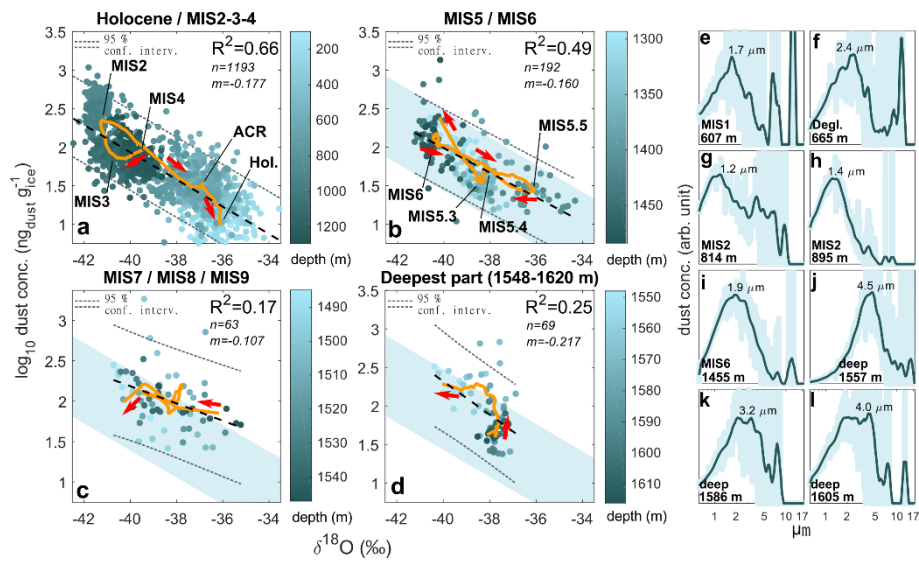
Figure 2. Panels a-d: linear correlation between $\delta^{18}O$ and dust concentration (logarithmic scale) in TALDICE. Dashed lines highlight the 95% confidence level interval of linear regression in each period; the blue band in panels b-d refers to the 95% confidence level interval of the linear regression calculated considering the last climatic cycle (panel a). The orange curve is the trajectory showing the evolution with time of the $\delta^{18}O$ - dust pair (arrows from deep to shallow). It was obtained applying a first order (40% sample window) Savitzky-Golay filter to both variables. Panel e-l: dust grain size distributions from TALDICE.

3.2. Major element composition of mineral dust

TALDICE dust composition during the last climatic cycle resembles the signature of Post Archean Australian Shale (PAAS, Taylor and McLennan, 1985; Fig. 3). With respect to the Upper Continental Crust (UCC, Rudnick and Gao, 2003), PAAS is

8

depleted in mobile oxides (such as CaO and Na_2O) and enriched in Fe- Ti- and Al-oxides as a result of chemical weathering. PAAS is in fact representative of surficial sedimentary rocks subject to chemical weathering (Taylor and McLennan, 1985), while UCC of the whole upper continental crust. The similarity between TALDICE dust and PAAS is not unexpected, since atmospheric dust is produced at the Earth surface, where sedimentary and weathered rocks dominate.

Another feature emerging from Fig. 3 is represented by the change of dust composition with depth (see also Fig. S4). The oxides showing the most evident trends are SiO_2 (increasing) and CaO (decreasing). Their average concentration varies between 64% and 1.7% in the Holocene to 74% and 0.4% in the deep part of the core, respectively. Other oxides showing minor variations are: Na_2O (decreasing), MgO (decreasing), Al_2O_3 (decreasing) and K_2O (increasing). These variations are related to depth and not to climatic cycles. This is an indication that they are likely related to post-depositional processes and not to primary changes of dust sources. A disturbance from the bedrock must be also discarded since the ice stratigraphy at Talos Dome is uninterrupted until 1548 m deep (Crotti et al., 2021). Ca, Mg and Na, the elements showing the strongest decrease, are mobile and typically affected by chemical weathering (Nesbitt & Young, 1982). Their reduction suggests a progressive alteration of dust with depth. In particular, the deepest samples lack MgO and CaO, indicating carbonate dissolution. The reaction between acidic species and carbonates and the consequent precipitation of gypsum, are well-known post-depositional processes in deep ice (Ohno et al., 2006; Iizuka et al., 2008; Traversi et al., 2009; Eichler et al., 2019). Our evidences suggest that this reaction also occurs at Talos Dome. The increase of SiO_2 is likely relative and reflects the progressive loss of labile species.
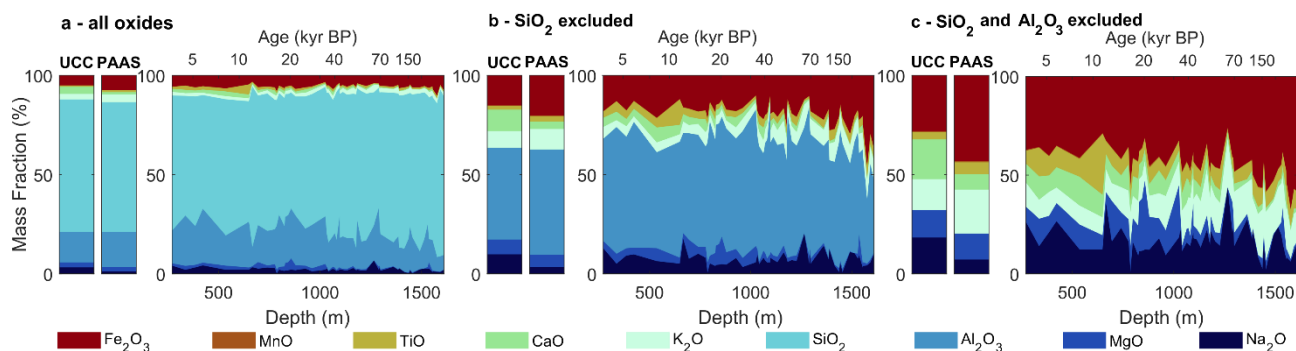
3.3. Iron oxidation and coordination symmetry

XANES reveals a progressive oxidation of Fe with depth (Fig. 4). Figure 4a shows that in the first 1000 m of the core, Fe in dust consists of a mixture of Fe^{2+} and Fe^{3+}, reflecting the typical composition of mineral aerosol (Schroth et al., 2009). Deep samples show a pure Fe^{3+} signature. About Fe-coordination, samples display an octahedral symmetry (coordination number 6), with secondary inputs from other geometries. This is also in accordance with observations concerning aerosols (Wilke et al., 2001; Formenti et al., 2014). Figure 4b shows the correlation between the energy of the pre-edge peak and of the K-edge transition, both related to Fe oxidation (Berry et al., 2003). Figure 4c shows the variation of the K-edge energy transition along the core. It increases by ~2 eV, pointing to the oxidation of Fe in mineral dust found in deep ice. The process is rather continuous, regardless of the climatic oscillations, suggesting that it relates to post-depositional changes. This is confirmed by the similarity of the oxidation trend and the growth of ice grains with depth (Fig. 4c). There are two exceptions: (1) in the deepest part of the core the Fe K-edge reaches a stable energy, pointing to a complete oxidation; (2) in correspondence with MIS2 and 4 the trend shows two slowdowns, as if oxidation is inhibited.

The partial increase of Fe^{2+} during glacial culminations is related to the transport of fresh glacial dust from South America (Spolaor et al., 2013), only partially oxidized due to limited atmospheric exposure (Shoenfelt et al., 2017). Another reason

Table 2. Average major element composition of TALDICE dust. Data are expressed as % mass fractions of oxides. For each climatic period mean values are reported with standard deviations.

Period	Holocene	Degl.	MIS2	MIS3	MIS4	MIS5	MIS6	deep part
(kyr BP)	0-11.7	11.7-19	19-31	31-58	58-68	68-132	132-154	154-unk.
Na_2O (m/m %)	3.1±1.1	2.1±1.0	1.9±0.5	2.0±0.5	4.3±3.3	2.3±1.0	0.2	1.6±0.9
MgO (m/m %)	1.6±0.4	2.0±1.0	3.0±1.6	0.8±0.3	0.8±1.1	0.4±0.3	0.5	0.6±0.8
Al_2O_3 (m/m %)	20.7±5.3	19.7±4.8	23±2.5	16.3±3.9	23.5±8.3	14.7±3.9	17.2	13.5±5.3
SiO_2 (m/m %)	63.9±5.0	65.9±6.3	62.9±3.4	72±3.6	63.9±4.5	73.4±3.9	72.9	74.2±5.6
K_2O (m/m %)	1.6±0.3	1.8±0.5	1.7±0.3	2.0±0.4	2.6±1.7	2.3±0.5	2.5	2.4±0.5
CaO (m/m %)	1.7±0.4	1.3±0.5	1.0±0.4	0.9±0.4	0.4±0.2	0.4±0.2	0.3	0.4±0.3
TiO_2 (m/m %)	1.5±0.4	1.6±1.3	0.9±0.2	0.9±0.2	0.4±0.2	0.9±0.3	0.8	1.0±0.2
MnO (m/m %)	0.06±0.02	0.05±0.01	0.06±0.02	0.04±0.02	0.05±0.04	0.04±0.01	0.04	0.04±0.02
Fe_2O_3 (m/m %)	5.8±0.6	5.6±1.3	5.4±1.1	5.1±0.8	4.0±1.0	5.5±0.6	5.6	6.3±1.5

Figure 3. Major element in dust from TALDICE. Data are shown considering all major element oxides (panel a), excluding SiO_2 (panel b) and SiO_2 and Al_2O_3 (panel c). UCC and PAAS references are shown for comparison (Rudnick and Gao, 2003; Taylor and McLennan, 1985).

for the slowdown of Fe oxidation during glacials is that in these periods the enhanced dust deposition at Talos Dome acts as a buffer and partially neutralizes the acidity of ice, consuming reactive species, as proposed for the Dome Fuji and EDML ice cores (Ohno et al., 2005, 2006; Eichler et al., 2019), and inhibits dust oxidation. Figure 4c shows that the growth of ice grains is also temporarily inhibited during MIS2 probably because of grain boundary pinning by insoluble particles as

10
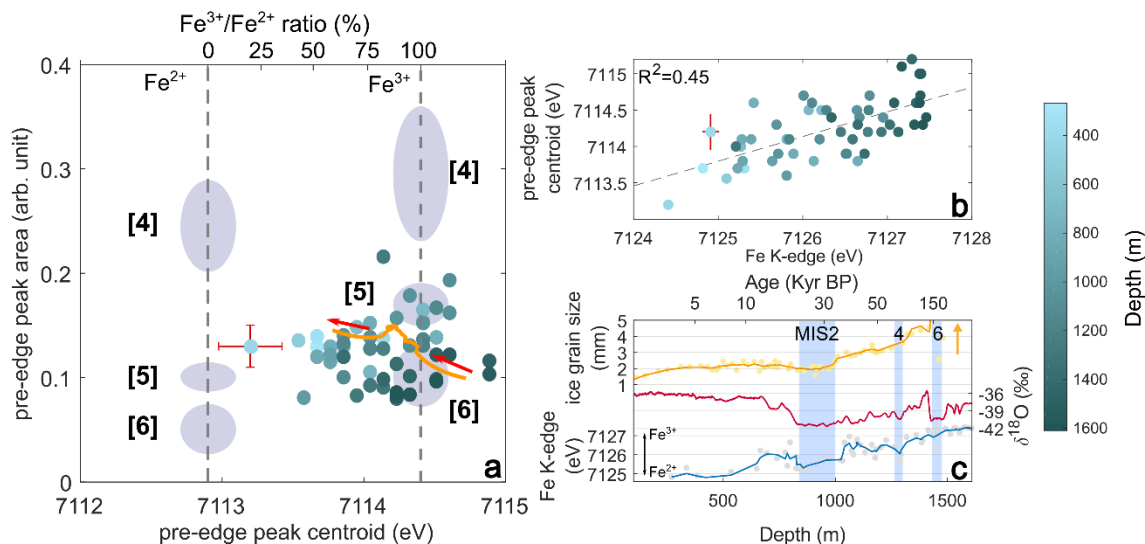
Figure 4. XANES results from the analysis of dust in TALDICE. Panel a: analysis of the Fe K- pre-edge spectral region. The intensity and energy position of the pre-edge peak are shown following the scheme proposed by Wilke et al. (2001). Ellipses and numbers in brackets refer to the coordination of Fe, vertical lines to its two oxidation states; the orange curve represents the trajectory of the samples along the core, it was calculated as in Fig. 2 (arrows from deep to shallow). Panel b: a comparison between the energy position of the pre-edge peak and the main K-edge transition (see Fig. S1 for details). Panel c: the energy position of the Fe K-edge transition (blue line) vs. isotope composition of ice (red line) (Stenni et al., 2011) and ice grain size (yellow line) (Montagnat et al., 2012); the arrow indicates the observed but not quantified ice crystals larger than 40 cm found below 1481 m deep); blue bands highlight MIS 2, 4 and 6. For each panel one point presents mean error bars (not visible in panel c because of scale).

suggested by Durand et al. (2006). A similar pattern is visible in MIS4, while ice corresponding to MIS6 does not present neither an Fe^{2+} recovery, nor a decrease of ice grain size (Figure 4c), probably because *in situ* oxidation of Fe-minerals and ice re-crystallization are too advanced. On the contrary, in interglacial ice atmospheric acidity is more available for post-depositional reactions favoring oxidation and weathering, also thanks to a more efficient ice re-crystallization (Iizuka et al., 2008; Eichler et al., 2019).

3.4. Iron mineralogy

Fe-mineralogy results are shown in Fig. 5, Fig. 6 and Tab. 3. Only minerals whose average relative abundance exceeds 2% have been considered in the discussion.

3.4.1. Hornblende and jarosite

Minerals showing the most evident trends are hornblende and jarosite. Hornblende dominates samples in the first 1000 m of TALDICE with a decreasing trend (Fig. 6a), on the contrary jarosite is present only below 1000 m deep and its concentration increases with depth (Fig. 6h). Trends related to these minerals involve large parts of the core regardless of climatic conditions; we interpret them as a consequence of post-depositional processes. Hornblende, $Ca_2(Fe^{2+}_4Al)(Si_7Al)O_{22}(OH)_2$, is

11

Table 3. Average relative abundance of Fe-bearing minerals in TALDICE dust. Data are expressed as % abundances.

Period	Holocene	Degl.	MIS2	MIS3	MIS4	MIS5	MIS6	deep part
(kyr BP)	0-11.7	11.7-19	19-31	31-58	58-68	68-132	132-154	154-unk.
Hornblende (%)	19.2	12.3	19.1	2.6	0	4.1	8.4	0.7
Muscovite (%)	11.5	12.9	18.0	13.0	7.6	2.0	0	0
Siderite (%)	2.9	3.9	0.4	4.2	1.9	2.1	0	1.1
Magnetite (%)	4.8	3.8	0	0.8	35.2	5.6	0	0.9
Goethite (%)	30.8	56.0	37.4	60.3	30.8	45.5	31.7	42.9
Hematite (%)	15.7	8.3	20.6	2.6	0	0	0	0
Pyrite (%)	5.9	1.8	0.5	1.8	3.3	1.9	1.7	2.1
Jarosite (%)	0	0	0	10.5	14.3	38.8	58.1	50.3
Others (%)	9.1	1.0	4.0	4.1	7.0	0	0	2.0

the second most abundant Fe-mineral in Holocene ice (relative abundance. 19%), but it rapidly decreases with depth and in the deepest part of TALDICE it is almost absent (relative abundance. 0.7%). Jarosite shows an opposite behavior. It is not

290 present in the shallow part of TALDICE, it appears below 1000 m deep, becoming the dominant Fe-bearing mineral below 1400 m (relative abundance. 50%). The two trends are linked. Hornblende is a common ferrous mineral present in South American dust (Shoenfelt et al., 2018) and is one of the dominant Fe^{2+}-bearing minerals in global aerosol (Schroth et al., 2009). Jarosite, $KFe_3(SO_4)_2(OH)_6$, is not common in atmospheric dust. It is well-known for being a weathering product and its widespread identification in the deep layers of TALDICE is regarded as evidence of weathering affecting dust in deep ice

295 (Baccolo et al., 2021). The concurrent decrease of hornblende and increase of jarosite confirm Fe oxidation. Hornblende seems to be the principal mineral whose dissolution leads to the consumption of Fe^{2+}, while jarosite build-up drives the accumulation of Fe^{3+}. The other minerals presenting a ferrous component, with the exception of magnetite, also show a decreasing trend (muscovite, siderite, pyrite) and are almost absent in the deepest part of the core.

3.4.2. Siderite and pyrite

300 Some minerals show a pattern in correspondence of MIS2, in some cases it is a relative maximum (muscovite, hematite), in others a minimum (siderite, pyrite). Considering the correspondence with MIS2, such features are interpreted as climate-related signals. In the Holocene siderite and pyrite, $FeCO_3$ and FeS_2 respectively, constitute about 3% each of Fe-minerals in TALDICE ice, but during MIS2 their abundance drop to 0.5%. A shift in mineralogy between the Holocene and MIS2 is expected, as in MIS2 dust is supplied to Talos Dome mostly by Patagonian sources (Delmonte et al., 2004, 2010), while in

305 the Holocene its origin is local from Northern Victoria Land (Delmonte et al., 2010; Baccolo et al., 2018b). The presence of siderite and pyrite in Holocene dust at Talos Dome agrees with the geology of Victoria Land, where they are common accessory minerals, owing to the basaltic/doleritic nature of local rocks (Sturm and Carryer, 1970; Dow and Neall, 1974). In addition to the geologic context, also atmospheric transport can partially explain their absence during MIS2. Both minerals
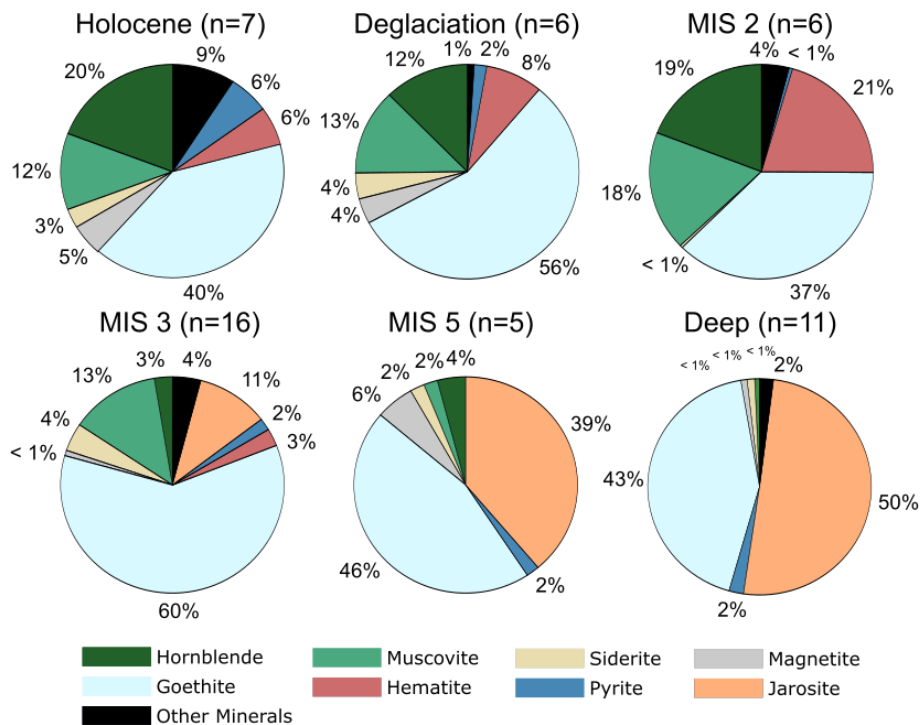
Figure 5. Pie-charts showing Fe-mineralogy of TALDICE dust. Each chart refers to a climatic period. Marine isotopic stages 4 and 6 have been excluded because of the low number of samples corresponding to these periods.

are easily oxidized when exposed to the atmosphere. Their lack in MIS2 can be related to their oxidation during the long-range transport from South America (Shi et al., 2012). On the contrary, in the Holocene siderite and pyrite did not undergo chemical reactions because of short-range atmospheric transport.

3.4.3. Muscovite

Muscovite reaches its highest relative abundance. during MIS2, presenting a mean value of 18%. Thanks to the aerodynamic shape of its crystals, muscovite, an Al-phyllosilicate, is common in atmospheric dust subject to long-range transport and is one of the most abundant minerals deposited on East Antarctica in MIS2 (Delmonte et al., 2017; Paleari et al., 2019). Its abundance in glacial ice is likely the main reason for the slowdowns observed along the oxidation trend of Fe (Fig. 4c), as Fe in muscovite is present as both ferric and ferrous iron. During MIS2 muscovite is the only mineral, with hornblende, presenting a ferrous component, since siderite, magnetite and pyrite are almost completely absent (Fig. 6). A similar pattern is observed in MIS4, when the second slowdown in Fe oxidation is observed, again corresponding to an increase of muscovite. In this second case both the slowing of oxidation and the increase of muscovite are less evident, probably because of the more advanced weathering at greater depth. Muscovite is completely absent below 1300 m deep, indicating that it is affected by weathering in deep ice, similarly to hornblende. Muscovite dissolution probably supplies a fraction of the K required for jarosite precipitation.

13
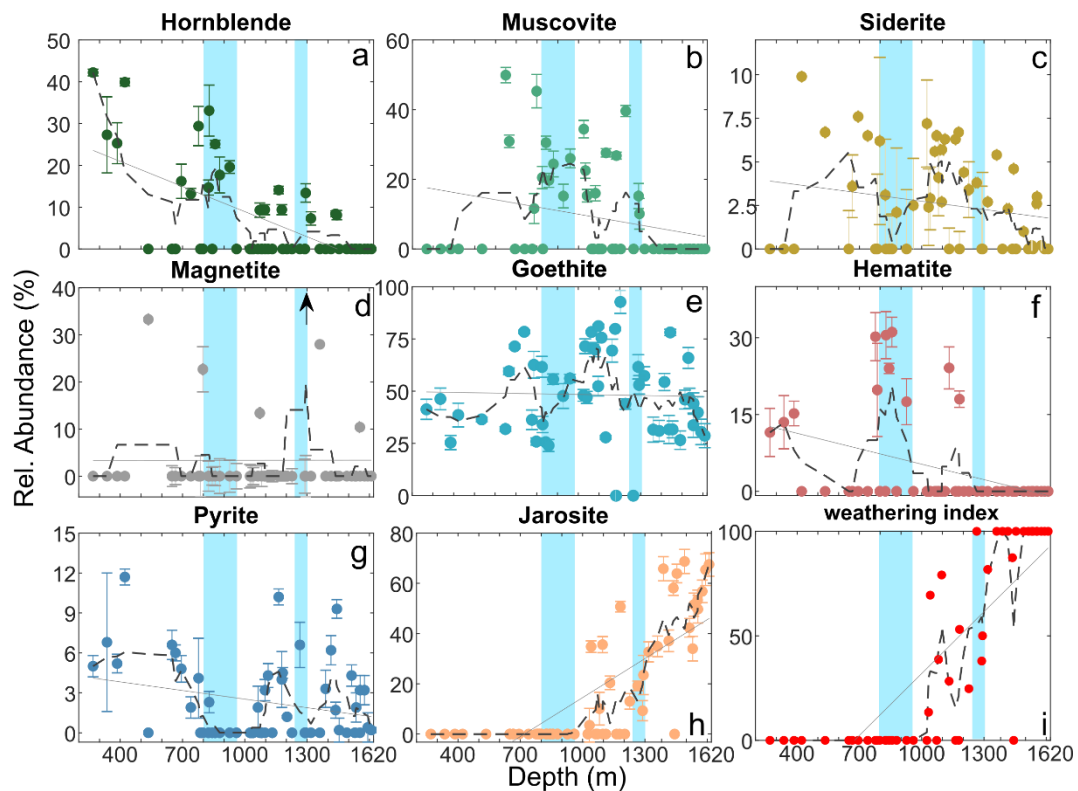
Figure 6. The variation of the major Fe-bearing minerals in TALDICE dust with depth. Dashed lines correspond to a 5-point moving average, solid grey lines to linear trends. In panel d, one sample-point is out of scale (black arrow, magnetite relative abundance. 70%). Panel i shows the weathering index, defined as the % ratio between jarosite concentration and the sum of jarosite, hornblende, muscovite and hematite.

3.4.4. Hematite

Hematite, Fe_2O_3, is a weathering product in soils under dry and warm conditions, it is typical in tropical regions while it is rarely encountered in cold and wet climates (Schwertmann, 1988). In TALDICE it is mostly found in MIS2, when the dust signature is fully South American (Delmonte et al., 2010). During glacial culminations an additional source other than Patagonia, the Puna-Altiplano dry region in the tropical Andes, supplies dust to Antarctica (Delmonte et al., 2010). In the Puna-Altiplano hematite is widely present (Aubry et al., 1996). Accordingly, our results show an excess of hematite in MIS2 (mean relative abundance. 21%). A previous study focusing on inner East Antarctica observes a higher abundance of hematite during the Holocene than in MIS2 (Paleari et al., 2019). The difference can be related to the geographic position of the two sites and to the influence of secondary sub-tropical sources during the Holocene. Below 1300 m deep, hematite is not observed, suggesting that this mineral is not stable in deep ice at Talos Dome. It is known that under acidic conditions (pH~4) hematite is not stable and dissolves (Schwertmann and Murad, 1983; Zolotov and Mironenko, 2007), leading to the precipitation of jarosite and goethite (Papike et al., 2006).

14

3.4.5. Goethite

Considering the entire core, goethite, FeO(OH), is the dominant Fe-mineral in dust, with a mean relative abundance. of 46% (the second is jarosite, 18% relative abundance.). The distribution of goethite with depth is rather uniform (Fig. 6e). This is indicative of the fact that (1) goethite is a common Fe-bearing phase in mineral aerosol (Formenti et al., 2014) and that (2) goethite is stable in the englacial environment, regardless of depth. The second point is corroborated by previous studies showing that at low temperature and in acidic wet environments, goethite is the most stable Fe oxide-hydroxide (Schwertmann and Murad, 1983; Zolotov and Mironenko, 2007).

3.4.6. Magnetite

Magnetite, Fe_3O_4, has a mean relative abundance. of about 3% and does not show evident trends; only a single sample presents a high concentration (70.4%). Without considering this anomalous value, possibly related to contamination or to the presence of a micrometeorite (Rochette et al., 2008), the mean value drops to 2%. Despite its low relative abundance., magnetite is relatively stable along TALDICE and it is not depleted in the deepest part, suggesting that it is not affected by oxidation and/or dissolution, as the other ferrous minerals considered in this study. This confirms its high chemical resistance to acidic oxidation (Moncur et al., 2009).

3.4.7. The weathering index

An index was developed to summarize the information from the different Fe-minerals. It is defined the weathering index and corresponds to the % ratio between the relative abundance. of jarosite and the sum between the relative abundance. of jarosite, hornblende, muscovite and hematite. The trend of the index varies between 0% in the upper part of TALDICE and 100% below 1300 m deep (Fig. 6i), reflecting the progressive weathering of dust, which consist in the consumption of some ferrous minerals and the precipitation of jarosite.

3.5. Englacial weathering of dust

When considering the pair Holocene-MIS2, which corresponds to the first 950 m of TALDICE, the chemical and physical properties of TALDICE dust are interpretable in the light of the well-known effects of major climatic swings on atmospheric dust. This is true for concentration, grain size and geochemistry. Below 1000 m deep, trends not related to climatic oscillations appear. The most evident is the increase of jarosite. The mineral is first observed at 1000 m deep, and its concentration increases toward the core bottom (Fig. 5 and Fig. 6h).

Jarosite is a Fe-K hydrated sulphate and results from chemical weathering. It has never been reported in global mineral aerosol. These features support the hypothesis that jarosite is a product of englacial diagenesis related to dust chemical weathering (Baccolo et al., 2021). Thanks to the conditions under which jarosite precipitates, its formation supplies information about the deep englacial environment. The precipitation of jarosite is an evidence for the presence of liquid

15

water in deep ice (pre-melting), since this mineral forms when limited amount of acidic (pH < 4) aqueous solutions rich in solutes (brines) interact with Fe-bearing minerals (Zolotov and Shock, 2005; Papike et al., 2006). At Talos Dome, ice temperature at 1000 m deep, where jarosite appears, is -25.5°C (Rix & Martin personal communication). Combining this information with the phase diagram of the sulfuric acid-water solution (Beyer et al., 2003), it is possible to estimate that acidic brines forming in deep ice at Talos Dome have a sulfuric acid concentration between 15 and 25% m/m. Liquid water in deep ice has been predicted by theories (Rempel et al., 2002; Marath and Wettlaufer, 2020; Ng, 2021) and confirmed by observations (Fukazawa et al., 1998). The englacial formation of jarosite is a further confirmation of deep ice pre-melting. Moreover, it is also indicative that liquid water found in deep ice is strongly acidic and oxidative.

The relationships between ice re-crystallization and the concentration of impurities in deep ice is not yet completely understood (Eichler et al., 2019; Stoll et al., 2021). Our study suggests that such correlation actually exists and that it has effects on dust geochemistry since Fe oxidation and ice grain growth share a similar trend in TALDICE (Fig. 4c). The formation of the acidic brines required for jarosite precipitation is in fact probably related to ice re-crystallization, since the latter has been invoked as the responsible for the concentration of impurities in localized environments and for the local lowering of pressure melting point (De Angelis et al., 2013; Tison et al., 2015;). The acidity of deep brines is explained in the light of the strong incompatibility of acidic atmospheric species with respect to the ice molecular lattice (Wolff, 1996) and of their concentration at grain boundaries (Mulvaney et al., 1988).

The formation of jarosite not only alters the original mineralogical assemblage of dust in TALDICE, but it can also be related to the anomalies in dust grain-size observed in deep ice (Figure 2e-l). Jarosite is known for creating a cementing matrix during weathering (Long et al., 1992). Its precipitation promotes the aggregation of mineral particles, altering the original grain size distribution. This has also been confirmed by microscopic observations, as shown in Baccolo et al., (2021). It is likely that chemical weathering also affects dust concentration, explaining the decrease of correlation with ice isotopic composition in the deep part of the ice core (Fig. 2).

Jarosite formation is not the only geochemical process occurring in deep TALDICE. Another anomaly is the oxidation of Fe present in dust (Fig. 4). The oxidation of Fe-minerals under acidic conditions is a well-known weathering pathway (Jones et al., 2014) which, among others, leads to jarosite precipitation (Papike et al., 2006). Fe oxidation is confirmed by the decline of many ferrous minerals in the deep part of the core (hornblende, muscovite, siderite and pyrite; see Fig. 5 and 6 and Tab. 3). The disappearance of hematite in deep TALDICE, which is not stable under acidic and wet conditions (Schwertmann and Murad, 1983), further supports oxidative/acidic weathering in deep ice at Talos Dome. The weathering index (Fig. 6i) summarizes these mineralogical changes and highlights the progressive weathering of dust with depth.

The trends of major element oxides in TALDICE dust (Tab. 2, Fig. 3) agree with the scenario described above. The decrease of Ca, Na and Mg with depth is interpreted as an effect of acidic weathering. In presence of acidic aqueous solutions, mobile

and soluble elements are easily mobilized (Nesbitt and Young, 1982). It is worth mentioning that Al oxide is also depleted in deep TALDICE dust. This suggests that also the most stable fractions of dust such as aluminosilicates, undergo weathering. This is confirmed by the identification in the deep part of the Dome Fuji ice core of secondary aluminum-sulphate (Ohno et al., 2014).

410

TALDICE presents a number of peculiarities if compared to other East Antarctic ice cores: deposition of local dust presenting a basaltic signature (Baccolo et al., 2018a), relatively warm temperatures, and a strong oceanic influence. Such features can explain why post-depositional processes affecting dust are so notable at this site. Basaltic-doleritic rocks are easily weatherable, even at low temperature (Li et al., 2016; Niles et al., 2017). In addition, Talos Dome is located near the

415   Southern Ocean and receives a considerable amount of marine aerosol rich in reactive acidic species (Iizuka et al., 2013; Mezgec et al., 2017). A further factor to consider is ice temperature. Talos Dome is located near the coast and its climate is tempered by the ocean. When considering the same depth, ice temperature at Talos Dome is about 15-20 °C warmer than at inner sites (Talalay et al., 2020) and temperature is an essential parameter for the relocation of impurities in deep ice (Marath and Wettlaufer, 2020).

420   All these local features are likely related to the ice-metamorphism observed in deep TALDICE (Montagnat et al., 2012), where ice crystals up to 40-50 cm have been observed below 1480 m deep. High ice-temperature and metamorphism could partially explain why dust alteration is so relevant in TALDICE, while at inner sites the original properties of dust seem preserved at greater depth and further back in time (Delmonte et al., 2004; Kawamura et al., 2017). Replicating this study at Inner Antarctic sites will be essential to distinguish the processes depending on the local characteristics of single sites from

425   the ones more deeply related to ice depth and age.

3.6. Conclusions and perspectives

This study provides a first description of dust chemical weathering in deep polar ice. Grain size, concentration, mineralogy and composition of dust are all affected by post-depositional processes in TALDICE. Fe speciation and mineralogy investigated through synchrotron radiation are efficient probes to explore such transformations in Antarctic ice. The

430   englacial precipitation of jarosite, the oxidation of Fe in dust, the decline of ferrous minerals (hornblende, pyrite, siderite, muscovite) and of hematite, and the depletion of some major elements (Ca, Mg, Na) suggest that below 1000 m deep, dust in TALDICE is affected by acidic-oxidative weathering. The latter results from the formation of acidic brines which interact with dust in deep ice, leading to geochemical reactions. The production of such brines is likely related to ice re-crystallization and to the accumulation of impurities in highly localized environments where the interaction between soluble

435   and insoluble species is favored. From this perspective deep Antarctic ice can be seen as a "geochemical reactor" capable of promoting the precipitation of secondary minerals and the dissolution of others. This study shows that dust-related signals in

ice cores, traditionally considered stable and resistant to post-depositional processes, are significantly altered in deep ice, at least in TALDICE.

It would be desirable to replicate the present study considering deep ice cores from inner East Antarctica where it would be possible to unveil additional processes related to the conditions found 2000-3000 m deep in the ice. Another possible implementation is the concurrent analysis of soluble and insoluble impurities, including elements other than Fe. This will help to investigate the dissolution and precipitation of primary and secondary minerals and identify the geochemical reactions responsible for these transformations, paving the way for the development of englacial geochemistry.

Author contributions. GB conceived the idea of this work. GB, BD, EDS prepared the samples and performed Coulter counter analyses. GB, GC, DH, AM carried out X-ray absorption and fluorescence analyses. GB interpreted the data and wrote the manuscript with contributions from all the coauthors.

Competing interests. The authors declare no competing interests.

References

Albani, S., Delmonte, B., Maggi, V., Baroni, C., Petit, J.-R., Stenni, B., Mazzola, C., and Frezzotti, M.: Interpreting last glacial to Holocene dust changes at Talos Dome (East Antarctica): implications for atmospheric variations from regional to hemispheric scales, Climate of the Past, 8, 741–750, 2012a.

Albani, S., Mahowald, N. M., 400 Delmonte, B.,Maggi, V., and Winckler, G.: Comparing modeled and observed changes in mineral dust transport and deposition to Antarctica between the Last Glacial Maximum and current climates, Climate Dynamics, 38, 1731–1755, 2012b.

Aubry, L., Roperch, P., de Urreiztieta, M., Rossello, E., and Chauvin, A.: Paleomagnetic study along the southeastern edge of the Altiplano- Puna Plateau: Neogene tectonic rotations, Journal of Geophysical Research: Solid Earth, 101, 17 883–17 899, 1996.

Baccolo, G., Cibin, G., Delmonte, B., Hampai, D., Marcelli, A., Di Stefano, E., Macis, S., and Maggi, V.: The contribution of synchrotron light for the characterization of atmospheric mineral dust in deep ice cores: preliminary results from the talos dome ice core (east antarctica), Condensed Matter, 3, 25, 2018a.

Baccolo, G., Delmonte, B., Albani, S., Baroni, C., Cibin, G., Frezzotti, M., Hampai, D., Marcelli, A., Revel, M., Salvatore, M., et al.: Regionalization of the atmospheric dust cycle on the periphery of the East Antarctic ice sheet since the last glacial maximum, Geochemistry, Geophysics, Geosystems, 19, 3540–3554, 2018b.

Baccolo, G., Delmonte, B., Niles, P. B., Cibin, G., Di Stefano, E., Hampai, D., Keller, L.,Maggi, V.,Marcelli, A.,Michalski, J., et al.: Jarosite formation in deep Antarctic ice provides a window into acidic, water-limited weathering on Mars, Nature Communications, 12, 1–8, 2021.

Barnes, P., Wolff, E., Mader, H., Udisti, R., Castellano, E., and Röthlisberger, R.: Evolution of chemical peak shapes in the Dome C, Antarctica, ice core, Journal of Geophysical Research: Atmospheres, 108, 2003.

Bazin, L., Landais, A., Lemieux-Dudon, B., Kele, H. T. M., Veres, D., Parrenin, F., Martinerie, P., Ritz, C., Capron, E., Lipenkov, V., et al.: An optimized multi-proxy, multi-site Antarctic ice and gas orbital chronology (AICC2012): 120-800 ka, Climate of the Past, 9, 1715–1731, 2013.

Berry, A. J., O'Neill, H. S. C., Jayasuriya, K. D., Campbell, S. J., and Foran, G. J.: XANES calibrations for the oxidation state of iron in a silicate glass, American Mineralogist, 88, 967–977, 2003.

Beyer, K. D., Hansen, A. R., and Poston, M.: The search for sulfuric acid octahydrate: experimental evidence, The Journal of Physical Chemistry A, 107, 2025–2032, 2003.

Burgay, F., Erhardt, T., Della Lunga, D., Jensen, C. M., Spolaor, A., Vallelonga, P., Fischer, H. and Barbante, C.: Fe2+ in ice cores as a new potential proxy to detect past volcanic eruptions, Science of the Total Environment, 654, 1110-1117, 2019.

Calvin, S.: XAFS for everyone. CRC Press, Taylor & Francis Group, 2013.

Cibin, G., Marcelli, A., Maggi, V., Baccolo, G., Hampai, D., Robbins, P. E., Liedl, A., Polese, C., D'Elia, A., Macis, S., et al.: Synchrotron Radiation Research and Analysis of the Particulate Matter in Deep Ice Cores: An Overview of the Technical Challenges, Condensed Matter, 4, 61, 2019.

Conway, T. M., Wolff, E. W., Röthlisberger, R., Mulvaney, R., and Elderfield, H.: Constraints on soluble aerosol iron flux to the Southern Ocean at the Last Glacial Maximum, Nature communications, 6, 1–9, 2015.

Crotti, I., Landais, A., Stenni, B., Bazin, L., Parrenin, F., Frezzotti, M., Ritterbusch, F., Lu, Z.T., Jiang, W., Yang, G.M., et al.: An extension of the TALDICE ice core age scale reaching back to MIS 10.1.Quaternary Science Reviews, 266, 107078, 2021.

De Angelis, M., Morel-Fourcade, M.-C., Barnola, J.-M., Susini, J., and Duval, P.: Brine micro-droplets and solid inclusions in accreted ice from Lake Vostok (East Antarctica), Geophysical Research Letters, 32, 2005.

De Angelis, M., Tison, J.-L., Morel-Fourcade, M.-C., and Susini, J.: Micro-investigation of EPICA Dome C bottom ice: evidence of long term in situ processes involving acid–salt interactions, mineral dust, and organic matter, Quaternary Science Reviews, 78, 248–265, 2013.

Delmonte, B., Petit, J., and Maggi, V.: Glacial to Holocene implications of the new 27000-year dust record from the EPICA Dome C (East Antarctica) ice core, Climate Dynamics, 18, 647–660, 2002.

Delmonte, B., Basile-Doelsch, I., Petit, J.-R., Maggi, V., Revel-Rolland, M., Michard, A., Jagoutz, E., and Grousset, F.: Comparing the Epica and Vostok dust records during the last 220,000 years: stratigraphical correlation and provenance in glacial periods, Earth-Science Reviews, 66, 63–87, 2004.

Delmonte, B., Baroni, C., Andersson, P. S., Schoberg, H., Hansson, M., Aciego, S., Petit, J.-R., Albani, S., Mazzola, C., Maggi, V., et al.: Aeolian dust in the Talos Dome ice core (East Antarctica, Pacific/Ross Sea sector): Victoria Land versus remote sources over the last two climate cycles, Journal of Quaternary Science, 25, 1327–1337, 2010.

Delmonte, B., Paleari, C. I., Andò, S., Garzanti, E., Andersson, P. S., Petit, J. R., Crosta, X., Narcisi, B., Baroni, C., Salvatore, M. C., et al.: Causes of dust size variability in central East Antarctica (Dome B): Atmospheric transport from expanded South American sources during Marine Isotope Stage 2, Quaternary Science Reviews, 168, 55–68, 2017.

Dow, J. and Neall, V.: Geology of the lower Rennick Glacier, northern Victoria Land, Antarctica, New Zealand Journal of Geology and Geophysics, 17, 659–714, 1974.

Durand, G., Weiss, J., Lipenkov, V., Barnola, J., Krinner, G., Parrenin, F., Delmonte, B., Ritz, C., Duval, P., Röthlisberger, R., et al.: Effect of impurities on grain growth in cold ice sheets, Journal of Geophysical Research: Earth Surface, 111, 2006.

Eichler, J., Weikusat, C., Wegner, A., Twarloh, B., Behrens, M., Fischer, H., Hörhold, M., Jansen, D., Kipfstuhl, S., Ruth, U., et al.: Impurity analysis and microstructure along the climatic transition from MIS 6 into 5e in the EDML ice core using cryo-Raman microscopy, Frontiers in Earth Science, 7, 20, 2019.

Faria, S. H., Freitag, J., and Kipfstuhl, S.: Polar ice structure and the integrity of ice-core paleoclimate records, Quaternary Science Reviews, 29, 338–351, 2010.

20

Fischer, H., Severinghaus, J., Brook, E., Wolff, E., and Albert, M.: Where to find 1.5 million yr old ice for the IPICS" Oldest Ice" ice core, Climate of the Past, 2013.

Formenti, P., Caquineau, S., Chevaillier, S., Klaver, A., Desboeufs, K., Rajot, J. L., Belin, S., and Briois, V.: Dominance of
535   goethite over hematite in iron oxides of mineral dust from Western Africa: Quantitative partitioning by X-ray absorption spectroscopy, Journal of Geophysical Research: Atmospheres, 119, 12–740, 2014.

Frezzotti, M., Bitelli, G., De Michelis, P., Deponti, A., Forieri, A., Gandolfi, S., Maggi, V., Mancini, F., Remy, F., Tabacco, I. E., et al.: Geophysical survey at Talos Dome, East Antarctica: the search for a new deep-drilling site, Annals of Glaciology, 39, 423–432, 2004.

540   Fukazawa, H., Sugiyama, K., Mae, S., Narita, H., and Hondoh, T.: Acid ions at triple junction of Antarctic ice observed by Raman scattering, Geophysical Research Letters, 25, 2845–2848, 1998.

Goossens, T., Sapart, C. J., Dahl-Jensen, D., Popp, T., El Amri, S., and Tison, J.-L.: A comprehensive interpretation of the NEEM basal ice build-up using a multi-parametric approach., Cryosphere, 10, 2016.

Hooper, J., Mayewski, P., Marx, S., Henson, S., Potocki, M., Sneed, S., Handley, M., Gassò, S., Fischer, M., and Saunders,
545   K. M.: Examining links between dust deposition and phytoplankton response using ice cores, Aeolian Research, 36, 45-60, 2019.

Iida, A.: Synchrotron Radiation X-Ray Fluorescence Spectrometry, in: Encyclopedia of Analytical Chemistry, DOI: 10.1002/9780470027318.a9329, 2013.

Iizuka, Y., Horikawa, S., Sakurai, T., 470 Johnson, S., Dahl-Jensen, D., Steffensen, J. P., and Hondoh, T.: A relationship
550   between ion balance and the chemical compounds of salt inclusions found in the Greenland Ice Core Project and Dome Fuji ice cores, Journal of Geophysical Research: Atmospheres, 113, 2008.

Iizuka, Y., Delmonte, B., Oyabu, I., Karlin, T., Maggi, V., Albani, S., Fukui, M., Hondoh, T., and Hansson, M.: Sulphate and chloride aerosols during Holocene and last glacial periods preserved in the Talos Dome Ice Core, a peripheral region of Antarctica, Tellus B: Chemical and Physical Meteorology, 65, 20 197, 2013.

555   Jones, A. M., Griffin, P. J., Collins, R. N., and Waite, T. D.: Ferrous iron oxidation under acidic conditions–The effect of ferric oxide surfaces, Geochimica et Cosmochimica Acta, 145, 1–12, 2014.

Jones, T., Cuffey, K., White, J., Steig, E., Buizert, C., Markle, B., McConnell, J., and Sigl, M.: Water isotope diffusion in the WAIS Divide ice core during the Holocene and last glacial, Journal of Geophysical Research: Earth Surface, 122, 290–309, 2017.

560   Kawamura, K., Abe-Ouchi, A., Motoyama, H., Ageta, Y., Aoki, S., Azuma, N., Fujii, Y., Fujita, K., Fujita, S., Fukui, K., et al.: State dependence of climatic instability over the past 720,000 years from Antarctic ice cores and climate modeling, Science advances, 3, e1600 446, 2017.

Li, G., Hartmann, J., Derry, L. A.,West, A. J., You, C.-F., Long, X., Zhan, T., Li, L., Li, G., Qiu,W., et al.: Temperature dependence of basalt weathering, Earth and Planetary Science Letters, 443, 59–69, 2016.

565 Liu, S., Xiao, C., Du, Z., Marcelli, A., Cibin, G., Baccolo, G., Zhu, Y., Puri, A., Maggi, V., and Xu, W.: Iron Speciation in Insoluble Dust from High-Latitude Snow: An X-ray Absorption Spectroscopy Study, Condensed Matter, 3, 47, 2018.

Long, D., Fegan, N., McKee, J., Lyons, W., Hines, M., and Macumber, P.: Formation of alunite, jarosite and hydrous iron oxides in a hypersaline system: Lake Tyrrell, Victoria, Australia, Chemical Geology, 96, 183–202, 1992.

Macis, S., Cibin, G., Maggi, V., Baccolo, G., Hampai, D., Delmonte, B., D'Elia, A., and Marcelli, A.: Microdrop deposition
570 technique: Preparation and characterization of diluted suspended particulate samples, Condensed Matter, 3, 21, 2018.

Maher, B., Prospero, J., Mackie, D., Gaiero, D., Hesse, P. P., and Balkanski, Y.: Global connections between aeolian dust, climate and ocean biogeochemistry at the present day and at the last glacial maximum, Earth-Science Reviews, 99, 61–97, 2010.

Mahowald, N., Kohfeld, K., Hansson, M., Balkanski, Y., Harrison, S. P., Prentice, I. C., Schulz, M., and Rodhe, H.: Dust
575 sources and deposition during the last glacial maximum and current climate: A comparison of model results with paleodata from ice cores and marine sediments, Journal of Geophysical Research: Atmospheres, 104, 15 895–15 916, 1999.

Marath, N. K., and Wettlaufer, J. S.: Impurity effects in thermal regelation. Soft Matter, 16, 5886, 2020.

Markle, B. R., Steig, E. J., Roe, G. H., Winckler, G., and McConnell, J. R.: Concomitant variability in high-latitude aerosols, water isotopes and the hydrologic cycle, Nature Geoscience, 11, 853–859, 2018.

580 Mezgec, K., Stenni, B., Crosta, X., Masson-Delmotte, V., Baroni, C., Braida, M., Ciardini, V., Colizza, E., Melis, R., Salvatore, M., et al.: Holocene sea ice variability driven by wind and polynya efficiency in the Ross Sea, Nature communications, 8, 1–12, 2017.

Moncur, M., Jambor, J., Ptacek, C., and Blowes, D.: Mine drainage from the weathering of sulfide minerals and magnetite, Applied Geochemistry, 24, 2362–2373, 2009.

585 Montagnat, M., Buiron, D., Arnaud, L., Broquet, A., Schlitz, P., Jacob, R., and Kipfstuhl, S.: Measurements and numerical simulation of fabric evolution along the Talos Dome ice core, Antarctica, Earth and Planetary Science Letters, 357, 168–178, 2012.

Mulvaney, R., Wolff, E. W., and Oates, K.: Sulphuric acid at grain boundaries in Antarctic ice, Nature, 331, 247–249, 1988.

Nesbitt, H. and Young, G.: Early Proterozoic climates and plate motions inferred from major element chemistry of lutites,
590 nature, 299, 715–717, 1982.

Ng, F. S.: Pervasive diffusion of climate signals recorded in ice-vein ionic impurities, The Cryosphere, 15, 1787–1810, 2021.

Niles, P. B., Michalski, J., Ming, D. W., and Golden, D.: Elevated olivine weathering rates and sulfate formation at cryogenic temperatures on Mars, Nature communications, 8, 1–5, 2017.

Ohno, H., Igarashi, M., and Hondoh, 510 T.: Salt inclusions in polar ice core: Location and chemical form of water-soluble
595 impurities, Earth and Planetary Science Letters, 232, 171–178, 2005.

Ohno, H., Igarashi, M., and Hondoh, T.: Characteristics of salt inclusions in polar ice from Dome Fuji, East Antarctica, Geophysical Research Letters, 33, 2006.

Ohno, H., Iizuka, Y., Horikawa, S., Sakurai, T., Hondoh, T., and Motoyama, H.: Potassium alum and aluminum sulfate micro-inclusions in polar ice from Dome Fuji, East Antarctica, Polar Science, 8, 1–9, 2014.

600 Ohno, H., Iizuka, Y., Hori, A., Miyamoto, A., Hirabayashi, M., Miyake, T., Kuramoto, T., Fujita, S., Segawa, T., Uemura, R., et al.: Physicochemical properties of bottom ice from Dome Fuji, inland East Antarctica, Journal of Geophysical Research: Earth Surface, 121, 1230– 1250, 2016.

Paleari, C. I., Delmonte, B., Andò, S., Garzanti, E., Petit, J. R., and Maggi, V.: Aeolian Dust Provenance in Central East Antarctica During the Holocene: Environmental Constraints From Single-Grain Raman Spectroscopy, Geophysical Research

605 Letters, 46, 9968–9979, 2019.

Papike, J., Karner, J., and Shearer, C.: Comparative planetary mineralogy: Implications of martian and terrestrial jarosite. A crystal chemical perspective, Geochimica et Cosmochimica Acta, 70, 1309–1321, 2006.

Potenza, M., Albani, S., Delmonte, B., Villa, S., Sanvito, T., Paroli, B., Pullia, A., Baccolo, G., Mahowald, N., and Maggi, V.: Shape and size constraints on dust optical properties from the Dome C ice core, Antarctica, Scientific reports, 6, 1–9,

610 2016.

Ravel, B. and Newville, M.: ATHENA, ARTEMIS, HEPHAESTUS: data analysis for X-ray absorption spectroscopy using IFEFFIT, Journal of synchrotron radiation, 12, 537–541, 2005.

Rempel, A. W., Wettlaufer, J., and Waddington, E. D.: Anomalous diffusion of multiple impurity species: Predicted implications for the ice core climate records, Journal of Geophysical Research: Solid Earth, 107, ECV–3, 2002.

615 Rochette, P., Folco, L., Suavet, C., Van Ginneken, M., Gattacceca, J., Perchiazzi, N., Braucher, R., and Harvey, R.: Micrometeorites from the transantarctic mountains, Proceedings of the National Academy of Sciences, 105, 18 206–18 211, 2008.

Royer, A., De Angelis, M. and Petit, J. R.: A 30000 year record of physical and optical properties of microparticles from an East Antarctic ice core and implications for paleoclimate models, Climatic Change, 5, 381-412, 1983.

620 Rudnick, R. and Gao, S.: Composition of the continental crust, The crust, 3, 1–64, 2003.

Ruth, U., Barnola, J.-M., Beer, J., Bigler, M., Blunier, T., Castellano, E., Fischer, H., Fundel, F., Huybrechts, P., Kaufmann, P., et al.: "EDML1": a chronology for the EPICA deep ice core from Dronning Maud Land, Antarctica, over the last 150 000 years, Climate of the Past, 3, 475–484, 2007.

Sakurai, T., Ohno, H., Motoyama, H., and Uchida, T.: Micro-droplets containing sulfate in the Dome Fuji deep ice core,

625 Antarctica: findings using micro-Raman spectroscopy, Journal of Raman Spectroscopy, 48, 448–452, 2017.

Schroth, A. W., Crusius, J., Sholkovitz, E. R., and Bostick, B. C.: Iron solubility driven by speciation in dust sources to the ocean, Nature Geoscience, 2, 337–340, 2009.

Schwertmann, U.: Occurrence and formation of iron oxides in various pedoenvironments, in: Iron in soils and clay minerals, pp. 267–308, Springer, 1988.

630 Schwertmann, U. and Murad, 545 E.: Effect of pH on the formation of goethite and hematite from ferrihydrite, Clays and Clay Minerals, 31, 277–284, 1983.

23

Shi, Z., Krom, M. D., Jickells, T. D., Bonneville, S., Carslaw, K. S., Mihalopoulos, N., Baker, A. R., and Benning, L. G.: Impacts on iron solubility in the mineral dust by processes in the source region and the atmosphere: A review, Aeolian Research, 5, 21–42, 2012.

Shoenfelt, E. M., Sun, J., Winckler, G., Kaplan, M. R., Borunda, A. L., Farrell, K. R., Moreno, P. I., Gaiero, D. M., Recasens, C., Sambrotto, R. N., et al.: High particulate iron (II) content in glacially sourced dusts enhances productivity of a model diatom, Science advances, 3, e1700 314, 2017.

Shoenfelt, E. M., Winckler, G., Lamy, F., Anderson, R. F., and Bostick, B. C.: Highly bioavailable dust-borne iron delivered to the Southern Ocean during glacial periods, Proceedings of the National Academy of Sciences, 115, 11 180–11 185, 2018.

Spolaor, A., Vallelonga, P., Cozzi, G., Gabrieli, J., Varin, C., Kehrwald, N., Zennaro, P., Boutron, C., and Barbante, C.: Iron speciation in aerosol dust influences iron bioavailability over glacial-interglacial timescales, Geophysical Research Letters, 40, 1618–1623, 2013.

Stenni, B., Buiron, D., Frezzotti, M., Albani, S., Barbante, C., Bard, E., Barnola, J., Baroni, M., Baumgartner, M., Bonazza, M., et al.: Expression of the bipolar see-saw in Antarctic climate records during the last deglaciation, Nature Geoscience, 4, 46–49, 2011.

Stoll, N., Eichler, J., Hörhold, M., Shigeyama, W., and Weikusat, I.: A review of the microstructural location of impurities in polar ice and their impacts on deformation, Frontiers in Earth Science, 8, 658, 2021.

Sturm, A. and Carryer, S.: Geology of the region between the Matusevich and Tucker Glaciers, north Victoria Land, Antarctica, New Zealand Journal of Geology and Geophysics, 13, 408–435, 1970.

Sugden, D. E., McCulloch, R. D., Bory, A. J.-M., and Hein, A. S.: Influence of Patagonian glaciers on Antarctic dust deposition during the last glacial period, Nature Geoscience, 2, 281–285, 2009.

Talalay, P., Li, Y., Augustin, L., Clow, G. D., Hong, J., Lefebvre, E., Markov, A., Motoyama, H., and Ritz, C.: Geothermal heat flux from measured temperature profiles in deep ice boreholes in Antarctica, The Cryosphere, 14, 4021–4037, 2020.

Taylor, S. R. and McLennan, S. M.: The continental crust: its composition and evolution, Blackwell Scientific Pub., Palo Alto, CA, 1985.

Tison, J.-L., de Angelis, M., Littot, G., Wolff, E., Fischer, H., Hansson, M., Bigler, M., Udisti, R., Wegner, A., Jouzel, J., et al.: Retrieving the paleoclimatic signal from the deeper part of the EPICA Dome C ice core, The Cryosphere, 9, 1633–1648, 2015.

Traversi, R., Becagli, S., Castellano, E., Marino, F., Rugi, F., Severi, M., Angelis, M. d., Fischer, H., Hansson, M., Stauffer, B., et al.: Sulfate spikes in the deep layers of EPICA-Dome C ice core: Evidence of glaciological artifacts, Environmental science & technology, 43, 8737–8743, 2009.

Veres, D., Bazin, L., Landais, A., Toyé Mahamadou Kele, H., Lemieux-Dudon, B., Parrenin, F., Martinerie, P., Blayo, E., Blunier, T., Capron, E., et al.: The Antarctic ice core chronology (AICC2012): an optimized multi-parameter and multi-site dating approach for the last 120 thousand years, Climate of the Past, 9, 1733–1748, 2013.

665 Wegner, A., Fischer, H., Delmonte, B., Petit, J. R., Erhardt, T., Ruth, U., Svensson, A., Vinther, B. and Miller, H.: The role of seasonality of mineral dust concentration and size on glacial/interglacial dust changes in the EPICA Dronning Maud Land ice core, Journal of Geophysical Research-Atmosphere, 120, 9916-9931, 2013.

Wilke, M., Farges, F., Petit, P.-E., Brown Jr, G. E., and Martin, F.: Oxidation state and coordination of Fe in minerals: An Fe K-XANES spectroscopic study, American Mineralogist, 86, 714–730, 2001.

670 Wolff, E., Barbante, C., Becagli, S., Bigler, M., Boutron, C., Castellano, E., De Angelis, M., Federer, U., Fischer, H., Fundel, F., et al.: Changes in environment over the last 800,000 years from chemical analysis of the EPICA Dome C ice core, Quaternary Science Reviews, 29, 285–295, 2010.

Wolff, E. W.: Location, movement and reactions of impurities in solid ice, in: Chemical Exchange between the atmosphere and polar snow, pp. 541–560, Springer, 1996.

675 Wolff, E. W., Fischer, H., Fundel, F., Ruth, U., Twarloh, B., Littot, G. C., Mulvaney, R., Röthlisberger, R., De Angelis, M., Boutron, C. F., et al.: Southern Ocean sea-ice extent, productivity and iron flux over the past eight glacial cycles, Nature, 440, 491–496, 2006.

Zolotov, M. Y. and Mironenko, M. V.: Timing of acid weathering on Mars: A kinetic-thermodynamic assessment, Journal of Geophysical Research: Planets, 112, 2007.

680 Zolotov, M. Y. and Shock, E. L.: Formation of jarosite-bearing deposits through aqueous oxidation of pyrite at Meridiani Planum, Mars, Geophysical Research Letters, 32, 2005.